Progress in Oceanography 116 (2013) 142–153

Contents lists available at SciVerse ScienceDirect

Progress in Oceanography

journal homepage: www.elsevier.com/locate/pocean

What does cause the collapse of the Western Alboran Gyre? Results of an operational ocean model

José C. Sánchez-Garrido [a,*], Jesús García Lafuente [a], Enrique Álvarez Fanjul [b], Marcos García Sotillo [b], Francisco J. de los Santos [c]

[a] Physical Oceanography Group, University of Málaga, Campus de Teatinos s/n, 29071 Málaga, Spain
[b] Área de Medio Físico, Puertos del Estado, Avda. del Partenón 10, 28042 Madrid, Spain
[c] Autoridad Portuaria Bahía de Algeciras, Avda. de la Hispanidad 2, 11207 Algeciras, Cádiz, Spain

ARTICLE INFO

Article history:
Received 16 October 2012
Received in revised form 19 June 2013
Accepted 7 July 2013
Available online 20 July 2013

ABSTRACT

The stability of the mean state of the surface circulation of the Western Alboran Sea, characterized by a jet of Atlantic water (AJ) surrounding the Western Alboran Gyre (WAG), is investigated with a submesoscale-resolving operational ocean model. It is shown that this circulation state collapses through the interaction between the AJ-WAG system and a growing cyclonic eddy that arises close to the Spanish coast. This eddy develops as the WAG partially blocks the positive potential vorticity (PV) flux coming from the Strait of Gibraltar. It is found that tides increase the positive PV flux with respect to a non-tidal simulation, thus making the destabilization of the mean circulation state more likely. Atmospheric pressure driven flows are also shown to have the potential to destabilize the circulation by rising dramatically the PV flux within a time scale of some days. This provides an explanation as to why the circulation of the Western Alboran Sea exhibits more variability toward winter time, when meteorological fluctuations are enhanced.

1. Introduction

The classical picture of the Alboran Sea surface circulation is characterized by an incoming jet of Atlantic Water (AJ) exhibiting a wavelike path around two anticyclonic gyres; the Western and Eastern Alboran Gyres (WAG and EAG respectively; see Fig. 1). Further east the AJ progresses to the Mediterranean along the African coast (Algerian current), while to the north old Atlantic Water returns from the western Mediterranean after a long cyclonic pathway. The eastern extension of the AJ, the so-called Almeria-Oran front, acts as a barrier that isolates the Alboran Sea from this current.

The described circulation is an attempt to draw a steady state, as the actual circulation is highly variable. Numerous works have reported the absence of either the WAG or the EAG, of both, and even the presence of three simultaneous anticyclonic gyres (Lanoix, 1974; Vargas-Yáñez et al., 2002). Higher variability has been observed during autumn and winter (Vargas-Yáñez et al., 2002), but its cause is not very well understood yet. The understanding of this variability is of concern because it has noticeable physical and ecological implications; for instance, Bryden and Stommel (1982) suggested that the presence of an energetic WAG facilitates the ventilation of Western Mediterranean Deep Water through Gibraltar, a hypothesis that has been recently verified by Naranjo et al. (2012) by means of long-term temperature records collected over the seafloor of the Strait of Gibraltar. In addition, a number of studies reveal the presence of submesoscale vortices around the gyres (Tintoré et al., 1991; García Lafuente and Delgado, 2004), which are spots of high biological productivity due to the large vertical velocities involved.

Viúdez et al. (1998) built an extensive conceptual view of the mean surface circulation of the Western Alboran Sea and illustrated an example of its variability. A set of sea surface temperature (SST) images indicated the eastward migration of the WAG and the genesis of a new gyre. The key event that triggered the sequence was the decoupling between the AJ and the WAG. These two structures are said to be coupled because the WAG owes its existence to the input of new Atlantic Water (AW) provided by the AJ. It was put forward that part of this water enters the gyre with tidally-induced agestrophic pulses (internal tides are strongly nonlinear; see, e.g., Sánchez-Garrido et al., 2008) of the AJ as it enters the Alboran Sea, while a second source is the flow bifurcation that takes place where the AJ impinges against the African coast near Cape Three Forks (see Fig. 1). The renewal of AW allows the maintenance of the gyre pressure gradient against frictional forces. On the other hand, without the presence of the WAG the AJ would be deflected to the south by the Coriolis acceleration immediately after entering the Alboran Sea. Instead, the AJ veers to the north when it meets the WAG as a result of the process of geostrophic

* Corresponding author. Tel.: +34 952132849; fax: +34 952135555.
E-mail address: jcsanchez@ctima.uma.es (J.C. Sánchez-Garrido).

0079-6611/$ - see front matter © 2013 Elsevier Ltd. All rights reserved.
http://dx.doi.org/10.1016/j.pocean.2013.07.002

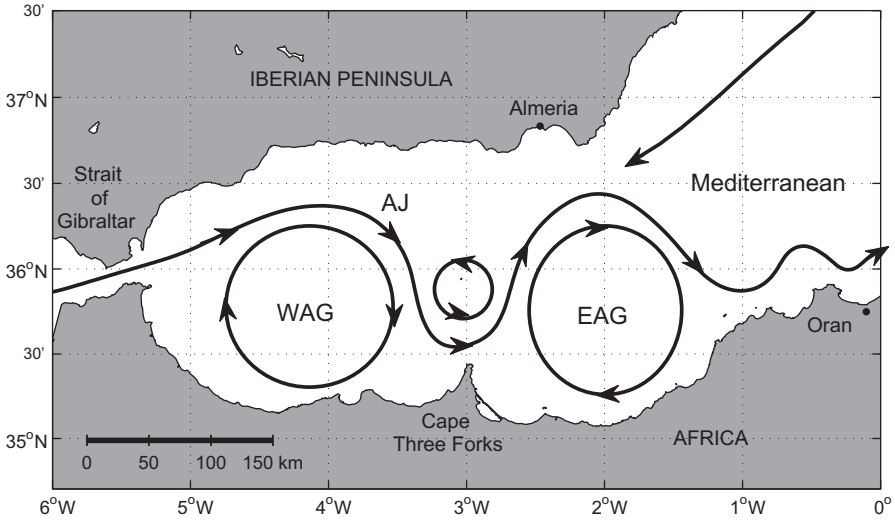

Fig. 1. Sketch of the classical surface circulation of the Alboran Sea. Contours represent stream lines. The Atlantic jet (AJ), the Western (WAG), and Eastern (EAG) Alboran gyres are labeled.

adjustment. Due to this feedback the two structures as whole are referred as to the AJ-WAG system.

Once the feedback between jet and gyre is established, it is not trivial to figure out how the system can be destabilized. Viúdez et al. (1998) explains the reported WAG migration event by an increase in size of the WAG and/or its northward displacement. This would force the AJ to flow eastwards instead of flowing in the usual north-east direction, thereby advecting the WAG to the east. As the WAG is sufficiently far from the strait the AJ has no longer to adjust geostrophically to the anticyclonic gyre, and consequently veers to the south due to the Coriolis acceleration. Its subsequent impingement against the African coast gives rise to a new WAG, which in turn displaces the old WAG further east. This process of gyre generation is well known and has been the topic of different experimental and numerical studies (see for instance Whitehead and Miller, 1979; Bormans and Garrett, 1989; Speich, 1996).

Vélez-Belchí et al. (2005) report a similar scenario and related the collapse of the AJ-WAG system with changes of the inflow conditions through the Strait of Gibraltar. It was argued that significant fluctuations of the inflow at subinertial scales, related to either atmospheric pressure driven flows or the fortnightly tidal signal, caused the WAG migration event. On the basis of an argument involving the inertial radius of curvature (u/f) they proposed that perturbations of the inflow velocities modify the AJ incident angle, with larger velocities leading to an AJ pointing to the center of the WAG and producing its eastwards advection. Flexas et al. (2006) revised these hypothesis by means of new satellite observations, and made some interpretations based on the quasi-geostrophic equation. However, their analysis was not conclusive.

This paper investigates the stability of AJ-WAG system and the circulation of the Western Alboran Sea. Differently to previous investigations, we make a numerical approach to the problem. We use a primitive-equation ocean model to investigate this issue. The model is a component of a recently implemented operational system of the Strait of Gibraltar and the Alboran Sea, and is described in Section 2. In Section 3 we present and discuss a sequence of SST images in which the AJ-WAG system collapses, while in Section 4 we analyse a series of sensitivity runs to investigate the likely mechanisms for triggering the event. Discussion and conclusions are included in Section 5.

2. Operational ocean circulation model

2.1. Model description

The operational ocean model is based on the Massachusetts Institute of Technology general circulation model (MITgcm). The MITgcm solves the Boussinesq form of the Navier–Stokes equations for an incompressible fluid with a spatial finite-volume discretization on a curvilinear computational grid. The model is free-surface, and has both a hydrostatic and a non-hydrostatic formulation (Marshall et al., 1997,).

The model domain covers the Gulf of Cadiz and the Alboran Sea (from 9.37°W to 1.59°E), and has been discretized with a curvilinear grid of variable resolution. Maximum horizontal resolution is reached within the Strait of Gibraltar with a cell size of about 400 m. With this resolution the strait contains about 30 grid cells across its narrowest section. Away from Gibraltar the resolution gradually decreases towards the open boundaries of the domain. In the area of special concern in this paper, the Western Alboran Sea, horizontal cell sizes are always less than 2800 m. The resolution is around the limits of applicability of the hydrostatic approximation. Nonetheless we adopt this approximation in our model because of the economy of the numerical code. The non-hydrostatic formulation requires the solution of a three-dimensional elliptic problem for the pressure field, which at present is computationally too expensive for the restricted computational time that the operational system demands. As a further improvement, the incorporation of non-hydrostaticity in the system is planned in the next future. In the vertical the model has 46 unevenly distributed z-levels with decreasing resolution from the ocean surface to the bottom. The first 20 levels are within the first 300 m of the water column. The bottom topography is obtained by merging the IOC (2003) 1-min resolution gridded bathymetry with a high-resolution bathymetic chart of the Strait of Gibraltar (Sanz et al., 1991). The bottom topography is represented by partial vertical cells in the model.

The subgrid-scale parametrisations and their respective parameter values are similar to those used by Sánchez-Garrido et al. (2011), who conducted a series of numerical experiments to study the generation process of nonlinear internal waves over the main sill of Gibraltar. Vertical diffusivity and viscosity are Richardson-

number dependent (Pacanowski and Philander, 1981). Horizontal eddy diffusivity is set to $k_h = 10^{-1}$ m^2 s^{-1}, whereas horizontal viscosity is calculated following the parametrization of Leith (1968).

The model is one-way nested to the MyOcean-MED large-scale Mediterranean model (hereinafter MyMED; Tonani et al., 2008; Oddo et al., 2009) through the open boundaries. Results from the MyMED model are used to force the two lateral open boundaries (west and east). Temperature, salinity, and velocity fields are interpolated from daily MyMED outputs and updated every time step. Note that MyMED does not include astronomical forcing, so the resulting net flow across the open boundaries consists of a subinertial meteorologically driven flow and a relatively small net flow (≈0.05 Sv) caused by the excess of evaporation over precipitation and run-off over the Mediterranean. Meteorologically driven flows are typically one order of magnitude greater than the net inflow caused by climate forcing, and because of their importance in modulating the exchange flow through Gibraltar (García Lafuente et al., 2002), have to be included in the system. However, MyMED can only partially simulate subinertial flows. It can reproduce wind-induced flows, but not subinertial flows related to changes in atmospheric pressure (atmospheric pressure forcing is not included in the model). As such, subinertial flows in our system are imported from the Nivmar storm surge forecast system based on a barotropic application of the HAMSOM model (Álvarez Fanjul et al., 2001; García Lafuente et al., 2002) covering the eastern Atlantic and the whole Mediterranean Sea. In order to prevent a double imposition of wind-induced flows coming from MyMED and Nivmar systems, velocity component normal to the open boundaries obtained from MyMED are corrected after interpolation by adding a (small) constant velocity value across the open-boundary sections so that zero net volume transport is finally prescribed.

Tidal forcing is also introduced by laterally forcing the model with barotropic tidal velocities derived from the Mog2d model (Carrere and Lyard, 2003). Thus, the final prescribed total velocity $\vec{u}_T$ can be written as:

$$\vec{u}_T(y,z,t) = \vec{u}_{MED}(y,z,t) + \vec{u}_{Niv}(y,t) + \vec{u}_{Tid}(y,t), \quad (1)$$

where $\int_{S_{obc}} \vec{u}_{MED}(y,z,t)dydz = 0$. Here $\vec{u}_{MED}, \vec{u}_{Niv}, \vec{u}_{Tid}$ are MyMED, Nivmar and tidal velocities respectively, and $\int_{S_{obc}}$ denotes integral across the open boundaries. Homogeneous Newman boundary condition is chosen for the free-surface, $\partial\eta/\partial n = 0$. Wave reflections at the open boundaries are minimized by adding a Newtonian relaxation term to the tracer equations over the boundary area and implementing the flow relaxation scheme proposed by Carter and Merrield (2007) for the velocity field.

At the sea surface, the model is driven by three-hourly values of wind stress, fresh water and heat surface fluxes provided by the Spanish Meteorological Agency through the operational Forecast System based on the HIRLAM model (Cats and Wolters, 1996). Downward shortwave and longwave radiation are provided directly from HIRLAM; upward longwave radiation is calculated from the model SST. Sensible and latent heat fluxes are calculated interactively using bulk formula, and evaporation is derived from the calculated latent heat flux. Since in the model evaporation typically exceeds precipitation, after some months of integration the sea level drops by few centimetres. This is prevented by using a mass flux correction to keep zero mean evaporation minus precipitation at every time step. No-slip condition is imposed at the solid boundaries.

The forecast bulletins of the model described here is daily updated and the outputs can be displayed at the official web site of Puertos del Estado through its ocean data view interface (Puertos del Estado, 2012). In this paper we consider two experiments. First, the ability of the model in reproducing the flow through the Strait of Gibraltar at different time scales is proved in a test run hindcasting the exchange flow in the period January–April 2010, when ADCP records are available. The second run covers the period September 15–November 30; 2011, and is aimed at reproducing the Alboran Sea surface circulation. Especial attention is paid to the variability of the WAG. The spin-up time is one month for the two experiments.

2.2. Model validation

First, the model surface tides are examined; then model velocities are compared with ADCP observations at the western end of the strait. Data were obtained from a monitoring station over Espartel Sill (ES; Fig. 2; 35°51.70′N, 5°58.60′W), equipped with an uplooking moored ADCP at 20 m above the seafloor (see García Lafuente et al., 2007, for further details).

The modeled co-tidal chart of the prevailing M_2 constituent (Fig. 2) has the known structure of tidal amplitudes abruptly decreasing from 90 cm to 30 cm within 0.5° distance as one moves from west of east, while phases have a transversal structure decreasing from south to north (García Lafuente et al., 1990). Modeled surface tides were compared with historical tidal gauge records at different locations of the strait (labeled in Fig. 2; see García Lafuente et al., 1990). It was found an overall satisfactory agreement, with, for instance, M_2 discrepancies smaller that 3 cm in amplitude and 10° in phase.

Fig. 3 depicts the subinertial variability of velocity over ES, both observed and as simulated by the model. The two time-series in question represent a two-layer flow structure with the interface oscillating around 190 m depth. The flow variability is induced by meteorological forcing, and is well reproduced by the model. Compare, for example, model and observations during events of noticeable reduction of the outflow (inflow intensification), when the interface of null velocity sinks below 200 m depth. These episodes occur in the two data sets in late June, February 8, and March 9, 24.

A quantitative comparison between the observed subinertial variability of the flow and simulated by the model is shown in Fig. 4, where the volume transport through ES cross section is plotted. Red and green lines correspond to an estimate of the Mediterranean outflow from ADCP observations and model outputs, respectively. For the comparison, we only consider the model velocity time series at the same place as the mooring station. The two time series are highly correlated, with similar mean values and variability. The computed transport from ADCP observations is −1.23 ± 0.37 Sv, while the model gives −1.37 ± 0.41 Sv. The most

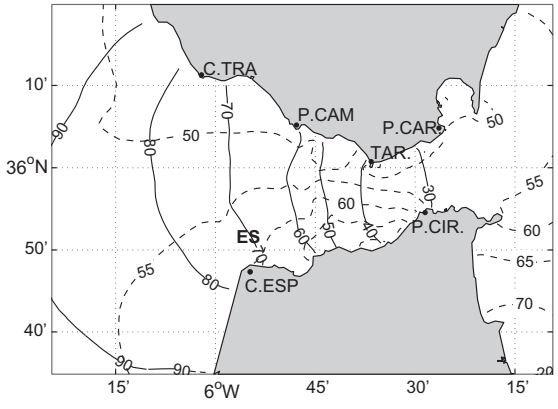

Fig. 2. Simulated co-tidal chart of the dominant M_2 tidal constituent in the Strait of Gibraltar. Solid and dashed lines are co-amplitude (cm) and co-phase lines, respectively. Several locations where historical sea level records exist are included in the map: Cape Trafalgar (C.TRA), Punta Camarinal (P.CAM), Tarifa (TAR), Punta Carnero (P.CAR), Punta Cires (P.CIR), and Cape Espartel (C.ESP). Label ES indicates the location of Espartel Sill.

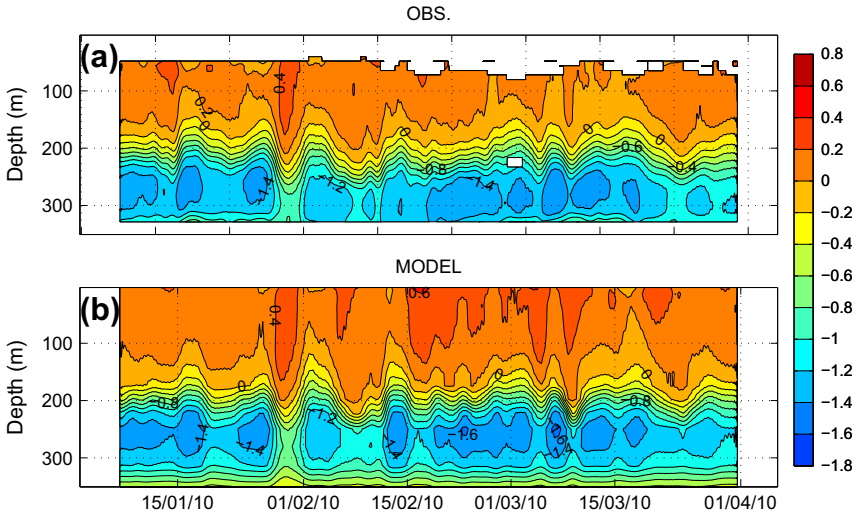

Fig. 3. (a) Subinertial ADCP zonal velocity time series over ES. A running Gaussian average filter with cut-off frequency of 48 h has been applied to the original time series. (b) Same as (a) with the modeled velocity.

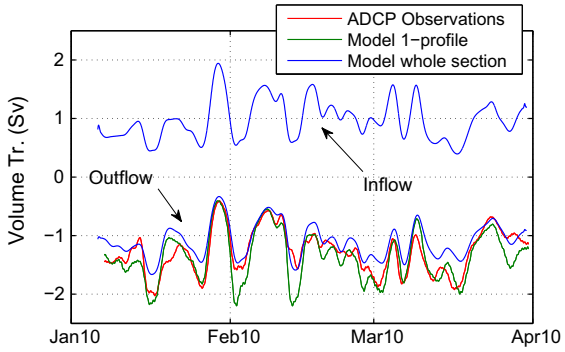

Fig. 4. Subinertial variability of the volume transport through ES. Red line: Mediterranean transport computed from ADCP observations. Green line: Mediterranean transport computed from the simulated velocity time series at the ADCP location. Blue line: modeled Atlantic/Mediterranean transport (integration across the whole ES cross-section). (For interpretation of the references to color in this figure legend, the reader is referred to the web version of this article.)

important discrepancies are found in the two outflow intensification events of early February, when the model overestimates the measured transport in ≈0.6 Sv. For comparison, the actual model transport (considering the whole ES section for the computation) has been also included in the Figure (blue line; the volume transport of the inflow is also included), and reveals that the 1-profile derived estimate overestimates the actual value (compare green and blue lines) of −1.1 ± 0.3 Sv, especially during episodes of outflow intensification. This is probably the effect of the decay of velocity towards the channel boundaries as a result of lateral friction.

3. Variability of the WAG during Autumn 2011

At the beginning of October 2011 SST imagery shows the classical configuration of the Alboran Sea surface circulation (Fig. 5a), with particularly large anticyclonic gyres. The gyres are distinguished in the image by warm cores, while new AW in the Alboran Sea is cooler. Modeled SST shows a very similar configuration (Fig. 5d). The model is successful in simulating the overall SST map, including some details as the strong cooling of surface water around the Strait of Gibraltar. The Almeria-Oran front and the Algerian current can be both distinguished in the SST maps. The only noticeable difference between the two pictures is the 1-degree model underestimation of SST to the north–east (southern limit of the Balearic Sea), away from the Alboran Sea.

Throughout the subsequent 8 days the WAG weakens as the cold signature of new AW spreads out over its northern edge (Fig. 5b and c). The WAG weakens further during the second part of October, and by the beginning of November it is nearly absent (Fig. 5h). At this time the incoming AW is warmer than the surface water of the Western Alboran Sea. At the eastern approach of Gibraltar warm water is found along the African coast, thus suggesting that the AJ is now pointing to the south-east. Eventually, within a period of only 5 days, a large WAG emerges from the coastal current (Fig. 5i). The whole sequence is successfully reproduced by the model (Fig. 5d–l), although with some slight mismatch in the timing.

Fig. 6 shows the daily mean sea surface velocity in the period of the WAG weakening. In a first stage the AJ points to its usual north–east direction under the presence of a well developed WAG (Fig. 6a). Within the next ten days a cyclonic vortex develops in the region between the AJ and the north coast, and grows in size until reaching a diameter of ≈70 km. Its western edge spreads over the eastern entrance of the strait and eventually deflects the AJ to the south (Fig. 6d). Over time the vortex and the jet form a mushroom-like current that progresses eastwards, thereby interacting with the WAG (Fig. 6d-e). Such a interaction results in a significant mass loss of the WAG (compare Fig. 6a and f), but even so, it still remains large enough to force the AJ to flow with a north-east component at the exit of the strait.

The definitive collapse of the AJ-WAG system occurs on October 24, when the AJ veers to the south and flows along the African coast (Fig. 7a). There the coastal current undergoes the already commented evolution: a fraction of the incoming AW keeps flowing eastwards along the coast, while other recirculates and develops an anticyclonic cell which is the seed of a new WAG. In this case this cell grows rapidly and within only 5 days becomes comparable to the old WAG (Fig. 7c). A number of works have reported at this stage an eastward migration of the old WAG due to its interaction with the new gyre (Viúdez et al., 1998;Vargas-Yáñez et al., 2002). In this case, however, the two gyres merge together into a new single WAG (Fig. 7d–f).

We have described a situation in which the AJ-WAG system collapses and the subsequent evolution of the surface circulation. However, the physical forcing behind the process and the mechanisms involved have not been investigated. All this is addressed in the next Section.

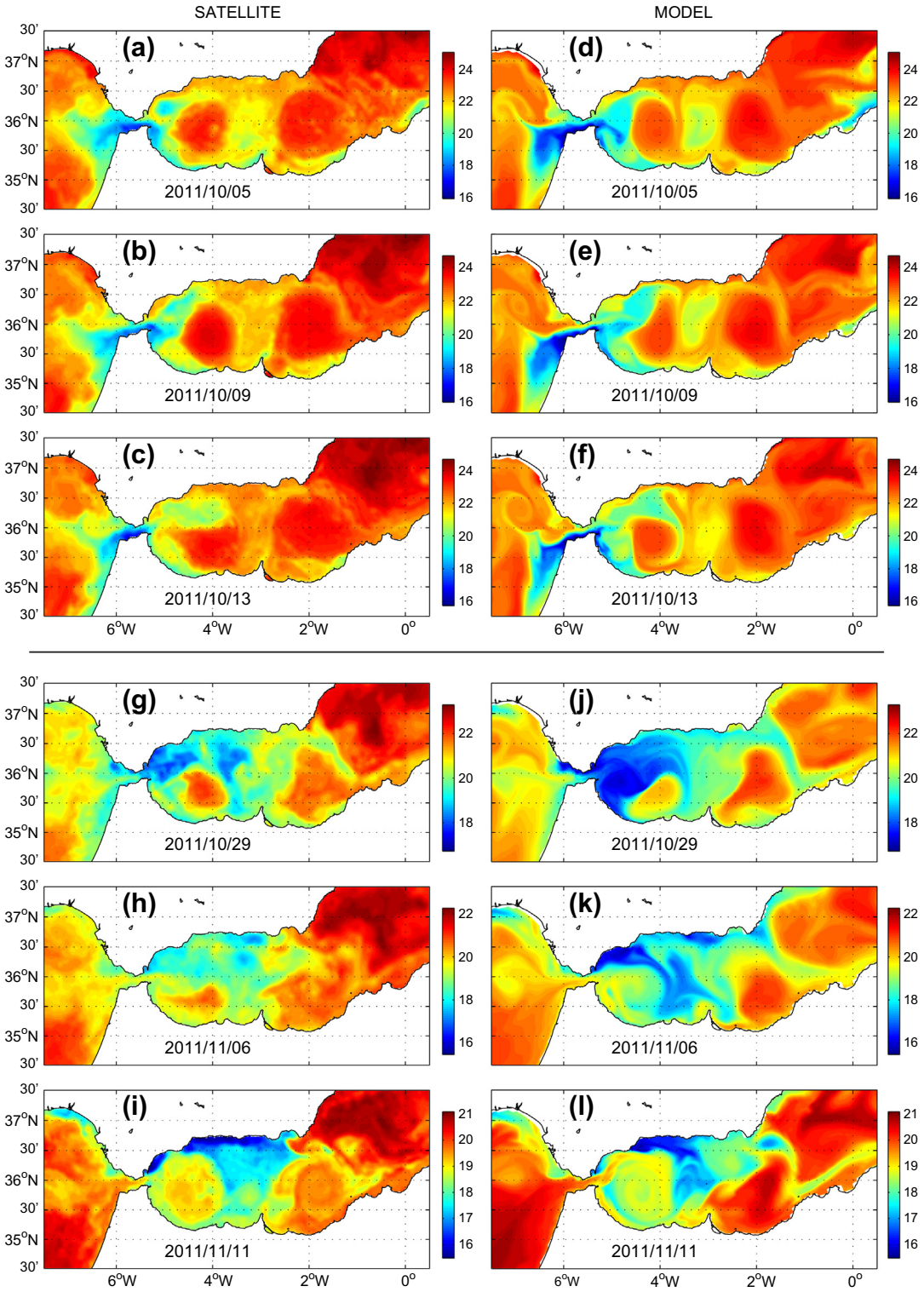

Fig. 5. Satellite (left column) and modeled (right column) daily mean SST time series of the Alboran Sea (units in °C). Note two different stages characterized by the weakening (panels a–f) and enhancement of the WAG (g–l).

4. Sensitivity runs

In order to gain insight into the problem, a set of sensitivity experiments isolating individual forcing has been conducted. In the first experiment (no external forcing, NEF) atmospheric (surface and lateral) and tidal forcings are turned off; across the open boundaries only the slowly-varying MyMED tracer and velocity fields (first term on the right hand side of Eq. (1)) force the model. The second run (TID) is as NEF but introducing tidal forcing (keeping the first and third terms on the right hand side of Eq. (1)). The third run (SUB) is as NEF but adding the remote meteorological forcing (keeping the first two terms on the right hand side of Eq.

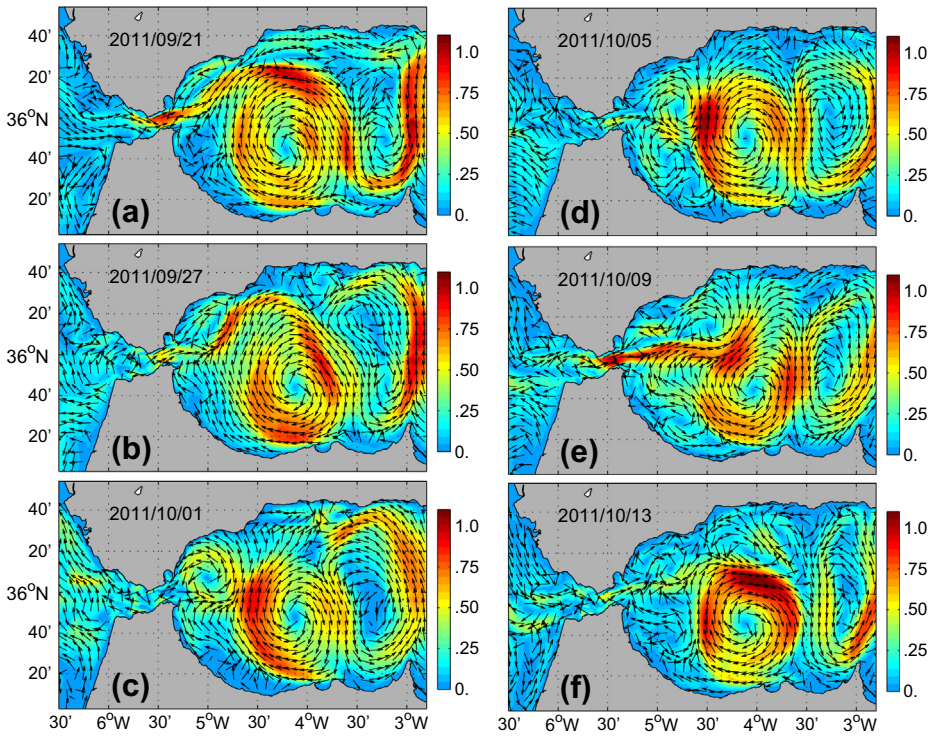

Fig. 6. Modeled daily mean surface velocity. Contours indicate velocity norm in m s^{-1}. Arrows indicate the flow direction (only a subset of the actual velocity vectors is shown).

(1)). Lastly, the MET run is as NEF but including surface atmospheric forcing.

4.1. NEF experiment

In this section we investigate the AJ-WAG system under nearly steady lateral forcing to elucidate whether it eventually collapses or, by contrast, reaches a quasi-steady state. The results reveal the occurrence of the later scenario. Throughout the 3-month run the AJ-WAG system maintains a steady configuration illustrated by Fig. 8a, which shows the time average sea surface heigh (SSH) obtained in the experiment.

Although the overall circulation pattern is nearly steady, it exhibits some variability that is worth to be mentioned. This vari-

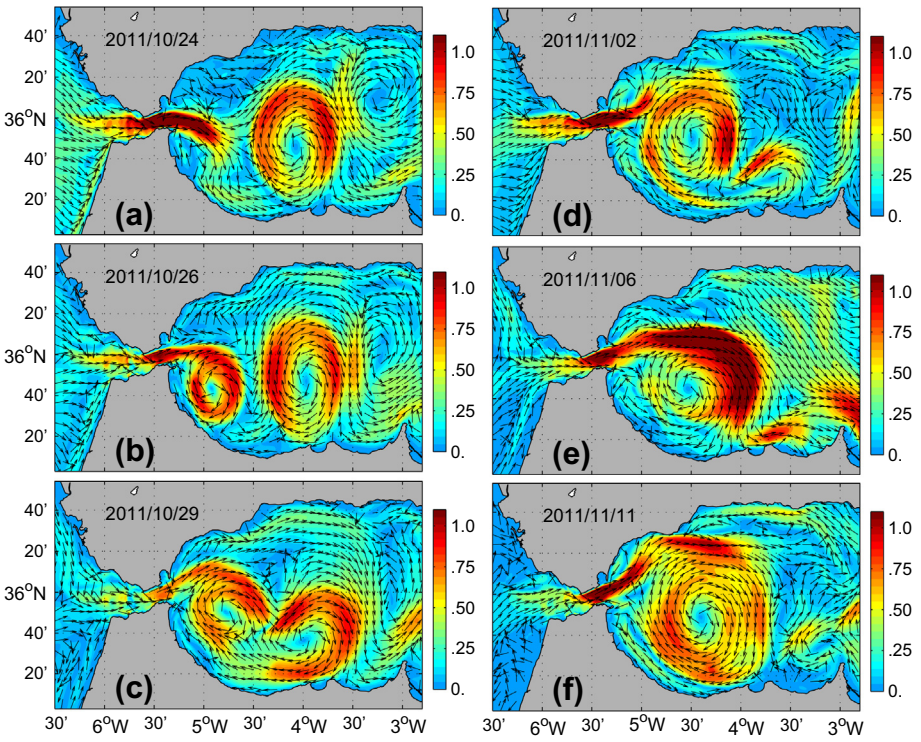

Fig. 7. Same as Fig. 6, for the period 2011/10/24–2011/11/11.

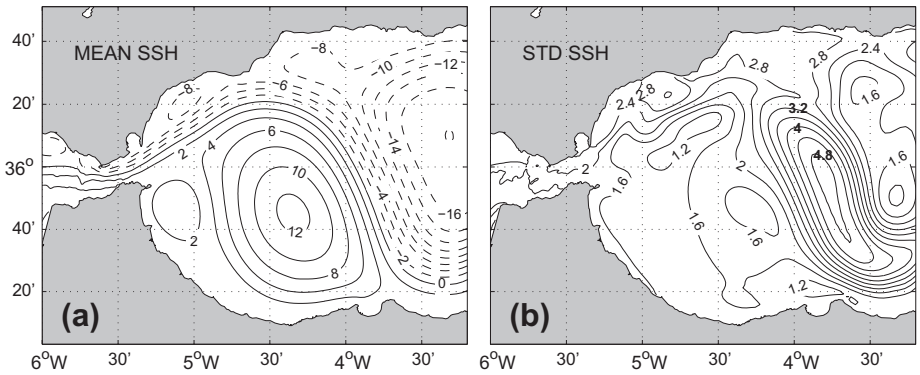

Fig. 8. Mean (a) and standard deviation (b) SSH values. The statistics are made on hourly SSH data obtained in the NEF simulation. Units are in cm. Solid and dashed lines indicate positive and negative values, respectively.

ability, given in terms of the standard deviation of SSH hourly data (Fig. 8b), is relatively low in the center of the gyre and increases in the area of the AJ. Inspection of surface velocity snapshots, like that shown in Fig. 9, indicates that this variability is introduced by the continuous meandering of the jet (note its wavy trajectory). Apparently, this behavior develops as the AJ enters the Alboran Sea and is later transmitted downstream.

Let us analyse the origin of the AJ meanders, as we anticipate here that it is closely related to the mechanism capable of triggering the collapse of the system. A feasible, and in fact common mechanism by which a jet meanders is the development of baroclinic instabilities (see e.g. Pedlosky, 1987; Mysak et al., 1981). While this mechanism might be at work here (the typical length scale of the meanders, $\lambda \approx 60$ km, and the internal Rossby radius, $r_i \approx 20$ km, are of the same order of magnitude), a dominant and more sophisticated effect emerges when monitoring the surface relative vorticity field. A snapshot time series of its vertical component ζ, normalized by the planetary vorticity f; or in other words, the Rossby number $Ro = \zeta/f$, is shown in Fig. 10. Along the central axis of the Strait of Gibraltar ζ is predominantly negative, and $Ro \approx -0.2$, sufficiently small for the flow to be considered nearly geostrophically balanced. This does not apply within two stripes of 2–3 km width along the strait's walls where $|Ro| > 1$; ζ is positive to the north and negative to the south. This pattern is the result of the high shear vorticity generated in the lateral boundary layers, which is later advected downstream. The important fact that flow separation from the lateral boundaries occurs periodically, especially from the south coast, favors the shedding of vortices to the Alboran Sea. The process is similar to the generation of Kármán vortex streets around blunt bodies that, in a geophysical context, has been observed around mountains and islands (see, e.g., Beggs et al., 2004). The periodic vortex shedding produces the AJ meanders.

Another noteworthy outcome of this experiment is that some of the released submesoscale ($Ro \approx 1$) anticyclonic vortices enter and merge with the WAG, thus becoming a source of new AW that helps to maintain the gyre pressure gradient.

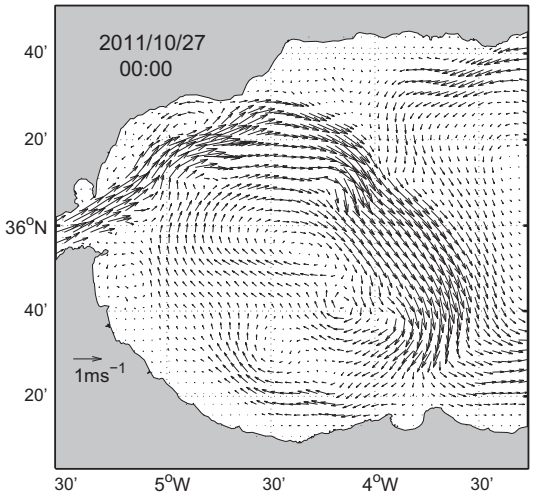

Fig. 9. Surface velocity snapshot corresponding to the NEF run (only a subset of the actual velocity vectors is shown). Time is 2011–10-27, 00:00 h.

4.2. TID experiment

The potential of tides for destabilizing the NEF circulation state is explored. Fig. 11a shows the surface vorticity field on September 22 and reveals a qualitatively similar pattern as in the NEF run; namely, high shear vorticity is produced on the strait's lateral boundaries, positive and negative to the north and south respectively, which is later advected towards the Alboran Sea. At some stage, however, a cyclonic vortex develops at the exit of the strait (≈5°W, 36°20′N; Fig. 11a) that remains trapped between the coast and the jet and gradually grows in size due to the continuous input of positive vorticity (Fig. 11b). After one week or so, it grows to such an extend that deflects the AJ to the south (Fig. 11c and d), much like in the original hindcast run. By October 13 (Fig. 12) the AJ points to the south-east and appears nearly decoupled to the WAG, and in a subsequent stage it runs completely along the African coast as the gyre migrates to the east (not shown). A new WAG does not emerge from the coastal current in this run.

This experiment demonstrates that tides have the potential to destabilize the AJ-WAG system by its own. This occurs through a process of accumulation of vorticity and vortex formation over the north western region of the Alboran Sea close to the strait. Therefore differently to the NEF run, the generated positive vorticity in the strait is not advected into the eastern Alboran sea in a continuous fashion. This can be explained by two facts: (1) the WAG is larger in this run than in NEF thus able to squeeze the AJ against the coast and block the positive vorticity flux; or (2) tides induce a greater vorticity flux no longer compatible with a WAG similar to the one in NEF.

The size of the gyre looks fairly similar in the two runs. A measure of it can be given in terms of the maximum SSH anomaly.[1] Indeed, in TID run this anomaly is about 1.5 cm greater than in NEF, which is a relatively small difference, ≈10%. While this difference might have contributed to the partial blocking of the positive vortic-

[1] anomaly with respect to the spatial average value.

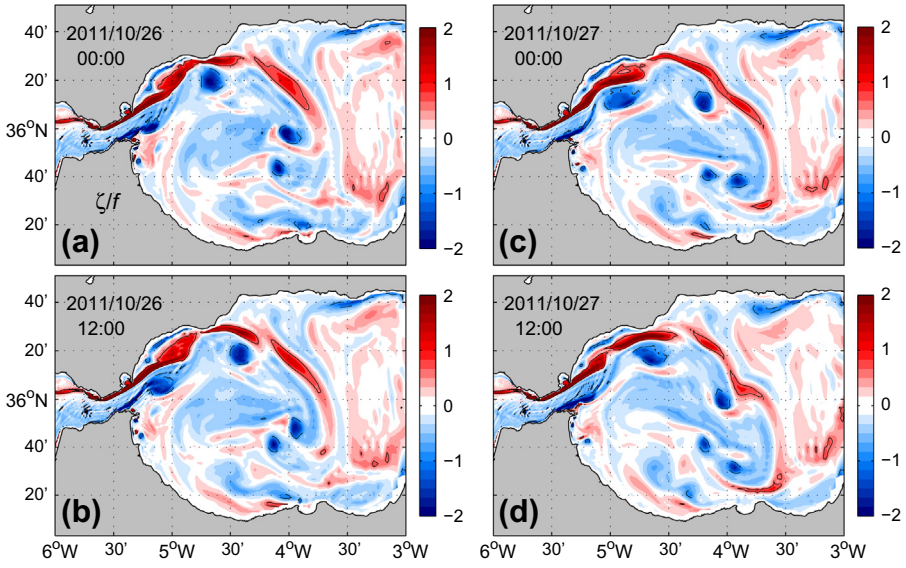

Fig. 10. Time series of surface relative vorticity (normalized values; ζ/f) obtained in the NEF run. $\zeta \approx 10f$ in the strait, but for the sake of clarity the color scale is set to $[-2,2]$. Solid and dashed contours are the isolines $\zeta/f = 3/4$ and $\zeta/f = -3/4$, respectively.

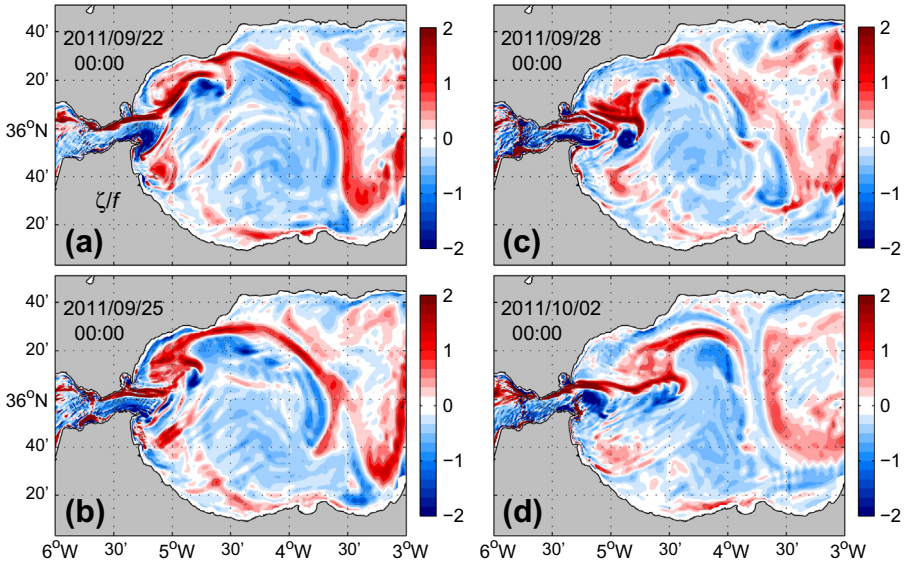

Fig. 11. Same as Fig. 10, for the TID run.

ity flux, it turns out that the main factor causing such blocking is a tidally-driven increase of the vorticity flux. To elaborate this, let us compare the potential vorticity (PV) transport through the strait in TID and NEF runs. PV is defined as in Marshall and Nurser (1992):

$$\mathrm{PV} \equiv Q = -\frac{1}{\rho}\omega \cdot \nabla\sigma, \tag{2}$$

where $\omega = 2\Omega + \nabla \times \vec{u}$ is the three-dimensional absolute vorticity, with Ω the angular velocity of the Earth; ρ denotes the sea water density, and σ the potential density anomaly (potential density minus 1000 kg m^{-3}). PV has units of m^{-1} s^{-1}, or pvs kg^{-1} if we define a "PV substance" (pvs) as 1 pvs = 1 kg m^{-1} s^{-1}. The PV flux (or transport) across a given section S is:

$$\mathrm{PVF} = \int_S \rho\, Q\, \vec{u} \cdot \hat{n}\, dS, \tag{3}$$

with $\hat{n}$ the surface unit normal vector. PVF has units of pvs s^{-1}.

Fig. 13 shows the PVF across the eastern exit of the Strait of Gibraltar (section S, see Fig. 12). Positive and negative values of PVF are shown separately. For the computation only the flow trough the Atlantic layer (layer above the pycnocline) has been considered. In the NEF simulation (thin solid line) the positive PVF exceeds by far the negative flux, with mean values of 2.46 and −0.15 pvs s^{-1}, respectively. This difference is attributable to the fact that the AJ is swifter towards the northern coast of the strait, thus with more potential to generate shear vorticity in that lateral boundary layer. As the flow is quasi-steady in this run, PVFs barely vary in time.

Now consider the tidal signal (thin gray line). Peak values of positive PVF are as large as 10 pvs s^{-1}, about four times as much the NEF flux. Negative PVF increases even more dramatically, from −0.15 to −4 pvs s^{-1}. Peaks are reached when the tidal flow causes the eastward acceleration of the AJ, whereas PVFs decay below NEF values as tidal currents reverse and the jet is slowed down. Note,

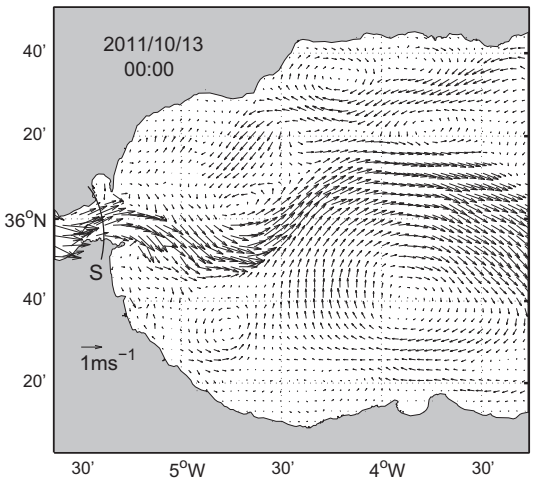

Fig. 12. Surface velocity snapshot corresponding to the TID run (only a subset of the actual velocity vectors is shown). Time is 2011–10-13, 00:00 h.

however, that the decay is not as pronounced as the increase, so that on average tides produce a net positive and negative PVF towards the Alboran Sea of 3.48 and -0.46 pvs s^{-1}, greater than in NEF run (thick gray line, Fig. 13).

4.3. SUB experiment

Tides modify significantly the input of PV from the strait to the Alboran Sea. It is expected that subinertial variations of the exchange flow modulate the PVF, and consequently be also of concern for the stability of the AJ-WAG system. This is investigated in this Section with the results of the SUB run.

As in TID, the positive PVF exhibits more variability than the negative flux (Fig. 13, dashed line). The positive PVF reaches peak values of around 5 pvs s^{-1} as the jet accelerates, while it becomes nearly null as it slows down. Differently to tides, subinertial flows do not introduce a residual PVF with respect to NEF run. This can be noted by the fact that $(\mathrm{PVF})_{\mathrm{SUB}}$ fluctuates rather symmetrically around $(\mathrm{PVF})_{\mathrm{NEF}}$ or, in other words, $\int (\mathrm{PVF})_{\mathrm{SUB}}\, dt = \int (\mathrm{PVF})_{\mathrm{NEF}}\, dt$ (areas under both curves in Fig. 13 are the same). Positive PVF in-

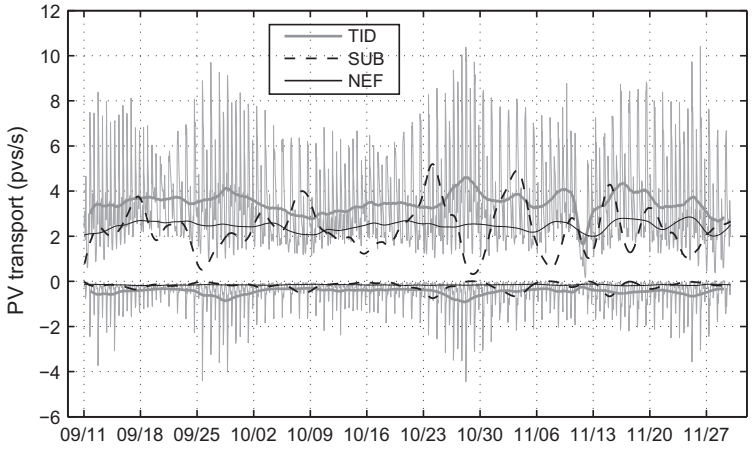

Fig. 13. PVF through the Strait of Gibraltar as obtained in NEF (solid line), TID (gray line), and SUB (dashed line) runs. The flux is for the Atlantic layer. Positive and negative fluxes are shown separately. The thick gray line is the low-passed tidal series.

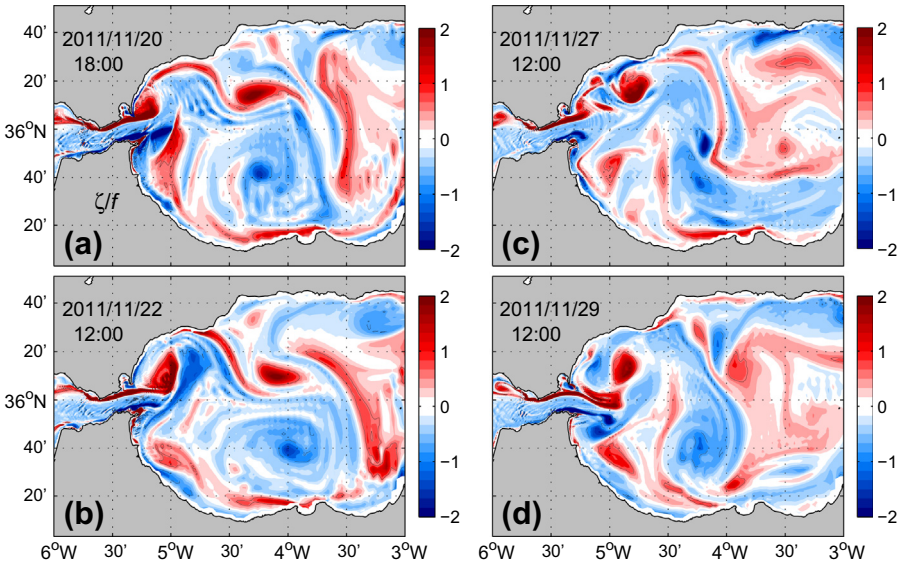

Fig. 14. Same as Fig. 10, for the SUB run.

duced by subinertial flows are smaller that those induced by tides, although are maintained in time for longer periods (some days against some hours), which has an striking effect as we shall see next.

Accelerations of the flow at subinertial scales and the associated generated vorticity give rise to vigorous submesoscale cyclonic vortices launched into the Alboran Sea. An example can be seen in Figs. 14 and 15 that show a time series of the surface vorticity and velocity fields by the end of November. The sequence is representative of the second part of the experiment when the flow variability is higher. As the AJ accelerates it enters the Alboran Sea adopting the shape of mushroom-like current (Fig. 14a, Fig. 15a). The sudden input of positive vorticity leads to the rapid development of a cyclonic submesoscale vortex to the northeast of the strait (Figs. 14b and 15b), similar to the one that is already surrounding the WAG by that time (≈4°15′W, 36°10′N; Figs. 14a and b, 15a and b). Several of these vortices were observed entering the eastern Alboran Sea throughout the simulation, but in this particular case the vortex gets trapped between the WAG and the coast for some days, and eventually breaks the link between the gyre and the jet (Fig. 15c and d). This demonstrates that subinertial flows have the potential to destabilize the system.

4.4. MET experiment

The last sensitivity run aims at studying the effect of surface atmospheric forcing on the circulation. It turns out that this effect is relatively weak as the AJ-WAG system results qualitatively unaffected during the simulation. The mean circulation state, given in terms of the time average SSH (Fig. 16), is quite similar to the one simulated in the NEF run (Fig. 8). The main difference concerns the WAG maximum SSH anomaly, now about 2 cm greater than in NEF. It is not our goal to provide an explanation for this here, but we speculate about the possibility that wind stress forcing might have driven a net ageostrophic flow into the gyre during the simulation.

While the mean SSH pattern does not change significantly with respect to NEF's, its variability pattern does (Fig. 16b). As expected, winds have increased the variability of the overall surface circulation. Although more variability is still observed along the jet path, the difference with the gyre is not as pronounced as in NEF, showing that wind stress has more influence on the gyre than on the jet, a fact further confirmed by the greater SSH anomaly maximum already commented.

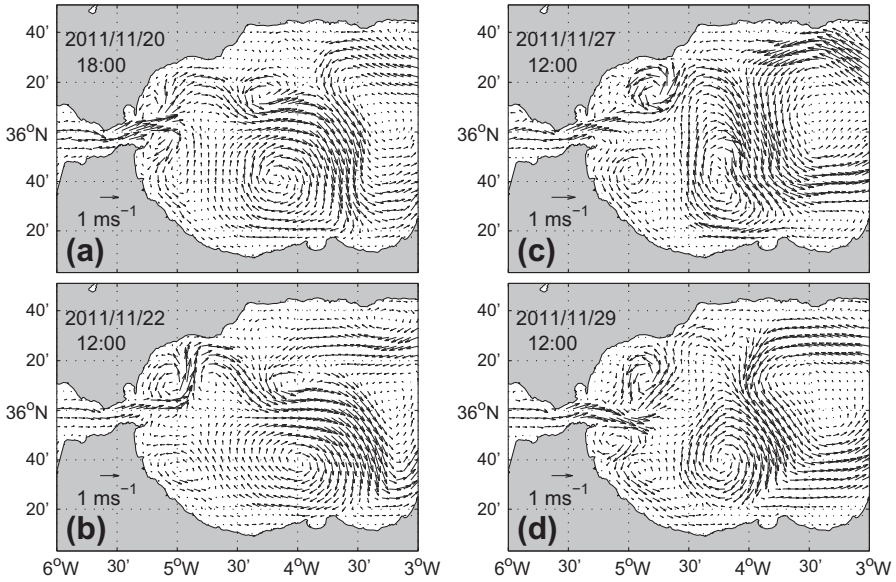

Fig. 15. Surface velocity time series by the end of the SUB experiment (only a subset of the actual velocity vectors is shown).

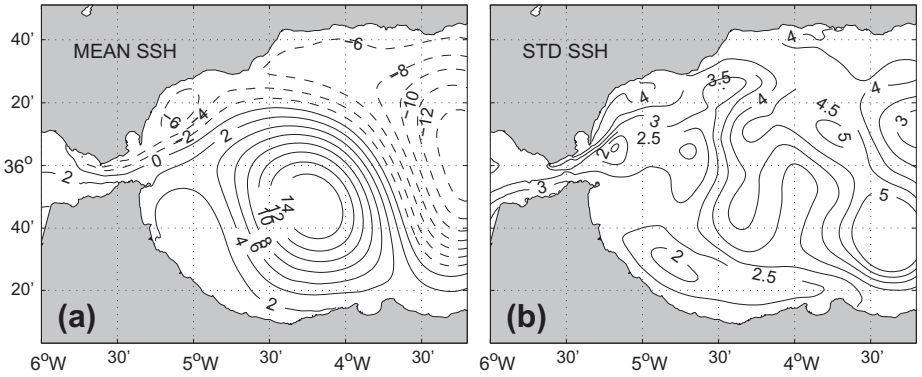

Fig. 16. Same as Fig. 8, for the MET run.

5. Discussion and conclusions

Many works in the literature have been devoted to the study of the Alboran Sea circulation and its variability, some of them speculating about the causes behind the collapse of the AJ-WAG system and the subsequent WAG migration. The hindcast run described here, carried out with an ocean model resolving the submesoscale dynamics in the Western Alboran Sea and driven by a comprehensive set of forcing, reproduced very satisfactorily the Alboran Sea SST variability during Autumn 2011. Motivated by this good performance of the model, we have used the model outputs and conducted additional sensitivity experiments to investigate the stability of the AJ-WAG system.

A recurrent feature observed in all experiments is the regular release of submesoscale vortices of either positive or negative vorticity from Gibraltar into the Alboran Sea, a process that resembles the generation of Kármán vortex streets from a solid body exposed to a uniform incident current. In this case, however, the process generating vorticity is the lateral friction within the lateral boundary layers along the north and south coasts of the strait where the AJ is noticeably ageostrophic. Positive and negative vorticities are generated in the north and south lateral boundary layers, respectively, and are later advected by the AJ into the Alboran Sea. This imported vorticity has proved to be an essential ingredient in the collapse of the AJ-WAG system.

Even when all the sensitivity experiments reproduce the vorticity advection, the runs differ from each other for the strength and the immediate fate of this vorticity in the Alboran Sea. In the NEF run, a quasi-steady circulation with a stable WAG is achieved. The submesoscale vortices, which are of reduced dimensions, are advected in a regular way by the AJ around the WAG until they are dissipated or merged with larger structures.

Tides have been shown to be able to break this circulation state. In fact, TID run shows that the AJ-WAG system breaks down at a similar timing as in the original hindcast run, which strongly suggests that tidal forcing was the main responsible for the collapse of the system. Tides generate much more shear vorticity than in NEF run (around 40% more on average but reaches peak values over four times greater), which in turn implies a great anomaly of positive PVF from the strait into the Northwestern Alboran Sea, that could take place in pulses associated with the tidal cycle. Under favorable conditions, this flux is partially blocked by the gyre and, as a result, a cyclonic vortex gradually emerges and grows in this area which finally breaks the link between AJ and WAG.

Subinertial flows (SUB run) also have the potential to break the system by essentially the same mechanism as tides although there is a subtle difference. PVF fluctuations in SUB run are smaller than in TID run but they last longer, giving them the chance of generating vigorous submesoscale cyclonic vortices in the Northwestern Alboran Sea in a time scale of some days. On the other hand it is worthy to mention that the average PVF in SUB run coincides with the NEF run but their fluctuations do not and this is the reason explaining why the former can reproduce the break of the AJ-WAG system and the latter cannot. It is the occurrence of large and relatively persistent subinertial fluctuations that has the potential to destabilize the AJ-WAG system, which in turn explains why the WAG shows less variability in summer when the meteorological forcing is less variable as well. Subinertial flow fluctuations enhance greatly in winter as cold fronts start to reach the Mediterranean area and increase the probability of the collapse of the AJ-WAG system. Consequently, the circulation in the Western Alboran Sea is indeed expected to exhibit more variability during this season.

The conclusion to be drawn from this description is that the joint action of subinertial fluctuations and tides increases largely the probability of collapse the AJ-WAG system, a probability that is even greater during spring tide periods. Notice, however, that even when meteorological forcing (SUB run) is able to destabilize the system, it is the TID run that better matches the timing of the AJ-WAG collapse observed in the original hindcast (and also in the SST sequence of infrared imagery, Fig. 5), which suggests that tides is the first candidate to trigger this kind of AJ-WAG instabilities.

To this regard it is important to say that the fact that tides have the potential to destabilize the circulation does not imply necessarily that the AJ-WAG system cannot hold for periods longer than one month, as suggested by the simulation presented here. Our model initialization leads to a relatively large WAG at the very beginning of the simulation. According to the above described processes, an initially smaller WAG would be much more stable as it has no chance to block the positive PVF coming from the strait. Until the WAG does not reach a critical size that allows for PVF blocking, the TID run will not show any AJ-WAG collapse and the Alboran Sea circulation will exhibit a rather stable pattern. At the other extreme and taking into account that significant positive PVF still exists in absence of tides, it is feasible that a sufficiently large (unrealistically large perhaps) initial WAG in the NEF run would have also collapsed over time. Therefore, tides must then be seen as a forcing under which the destabilization of the AJ-WAG system becomes more likely, and this is even more true if the subinertial variability is considered.

This study highlights the relevance of submeso and small-scale (less than 1 km) processes in driving the temporal variability of the Alboran Sea surface circulation. The processes are forced by tidal and atmospheric pressure driven flows (the main external agent of the subinertial variability of flows through the Strait). A conclusion is then that the modeling of a realistic variability of the Alboran Sea circulation demands the consideration of a fine computational grid and a very restrictive integration time step if surface gravity waves are to be resolved explicitly, which makes runs longer than those conducted here be computationally quite expensive.

Acknowledgments

The operational model described in this work was developed in the framework of the SAMPA Project, funded by Autoridad Portuaria de la Bahía de Algeciras and Puertos del Estado. Financial help from the Spanish-funded Project CTM2010-21229 is also acknowledge. This study has been conducted using MyOcean Products provided by the Italian INGV institute. We are thankful to Justo Conde from AEMET for facilitating the atmospheric forcing fields.

References

Álvarez Fanjul, E., Pérez Gómez, B., Rodríguez Sánchez, A.I., 2001. Nivmar: a storm surge forecasting system for Spanish waters. Scientia Marina 65 (S1), 145–154.
Beggs, P., Selkirk, P., Kingdom, D., 2004. Identification of Von Karman vortices in the surface winds of heard island. Boundary-Layer Meteorology 113, 287–297.
Bormans, M., Garrett, C., 1989. A simple criterion for gyre formation by the surface outflow from a strait, with application to the Alboran Sea. Journal of Geophysical Research 94 (C9), 12637–12644.
Bryden, H.L., Stommel, H., 1982. Origin of the mediterranean outflow. Journal of Marine Research 40, 55–71.
Carrere, L., Lyard, F., 2003. Modelling the barotropic response of the global ocean to atmospheric wind and pressure forcing – comparisons with observations. Geophysical Research Letters 30 (6), 1–8.
Carter, G.S., Merrield, M.A., 2007. Open boundary conditions for regional tidal simulations. Ocean Modelling 18, 194–209.
Cats, G., Wolters, L., 1996. The Hirlam project. International Journal of Computational Science and Engineering 3, 4–7.

Oddo, P., Adani, M., Pinardi, N., Fratianni, C., Tonani, M., Pettenuzzo, D., 2009. A nested atlantic-mediterranean sea general circulation model for operational forecasting. Ocean Science 5, 461–473.

Flexas, M., Gomis, D., Ruiz, S., Pascual, S., León, P., 2006. In situ and satellite observations of the eastward migration of the Western Alboran Sea gyre. Progress in Oceanography 70, 486–509.

García Lafuente, J., Almazán, JL., Fernández, F., Khribeche, A., Hakimi, A., 1990. Sea level in the strait of gibraltar: tides. International Hydrographic Review LXVII (1), 111–130.

García Lafuente, J., Álvarez Fanjul, E., Vargas, J.M., Ratsimandresy, A.W., 2002. Subinertial variability in the flow through the Strait of Gibraltar. Journal of Geophysical Research 107 (C10), 3168.

García Lafuente, J., Delgado, J., 2004. Meandering path of a drifter around the Western Alboran Gyre. Journal of Physical Oceanography 34 (3), 685–692.

García Lafuente, J., Sánchez Román, A., Díaz del Río, G., Sannino, G., Sánchez-Garrido, J.C., 2007. Recent observations of seasonal variability of the Mediterranean outflow in the Strait of Gibraltar. Journal of Geophysical Research 112, C10005. http://dx.doi.org/10.1029/2006JC003992.

IOC, IHO and BODC, 2003. Centenary Edition of the GEBCO Digital Atlas, published on CD-ROM on behalf of the Intergovernmental Oceanographic Commission and the International Hydrographic Organization as part of the General Bathymetric Chart of the Oceans. British Oceanographic Data Centre, Liverpool.

Lanoix, F., 1974. Project Alboran: Hydrologic and Dynamic Study of the Alboran Sea (in French). Tech. Rep. 66, N. Atl. Threaty Org., Brusels.

Leith, C.E., 1968. Diffusion approximation for two-dimensional turbulence. Physics of Fluids 10, 1409–1416.

Marshall, J., Nurser, A.G., 1992. Fluid dynamics of oceanic thermocline ventilation. Journal of Physical Oceanography 22, 583–595.

Marshall, J., Hill, C., Perelman, L., Adcroft, A., 1997. Hydrostatic, quasi-hydrostatic, and nonhydrostatic ocean modeling. Journal of Geophysical Research 102 (C3), 5733–5752.

Marshall, J., Adcroft, A., Hill, C., Perelman, L., Heisey, C., 1997. A finite-volume, incompressible Navier Stokes model for studies of the ocean on parallel computers. Journal of Geophysical Research 102 (C3), 5753–5766.

Mysak, L.A., Johnson, E.R., Hsieh, W.W., 1981. Baroclinic and Barotropic instabilities of coastal currents. Journal of Physical Oceanography 11, 209–230.

Naranjo, C., García-Lafuente, J., Sánchez-Garrido, J.C., Sánchez-Román, A., Delgado, J., 2012. The Western Alboran Gyre helps ventilate the Western Mediterranean Deep Water through Gibraltar. Deep Sea Research Part I 63, 157–163.

Pacanowski, R.C., Philander, S.G.H., 1981. Parameterisation of vertical mixing in numerical models of Tropical Oceans. Journal of Physical Oceanography 11, 1443–1451.

Pedlosky, J., 1987. Geophysical Fluid Dynamics. Springer Verlag, New York, 710pp.

Puertos del Estado, 2012. Ocean data view interface of Puertos del Estado. http://www.puertos. es/oceanografia_y_meteorologia/redes_de_medida/index.html.

Sánchez-Garrido, J.C., García Lafuente, J., Criado Aldeanueva, F., Baquerizo, A., Sannino, G., 2008. Time-spatial variability observed in velocity of propagation of the internal bore in the Strait of Gibraltar. Journal of Geophysical Research 113, C07034. http://dx.doi.org/10.1029/2007JC004624.

Sánchez-Garrido, J.C., Sannino, G., Liberti, L., García Lafuente, J., Pratt, L., 2011. Numerical modeling of three-dimensional stratified tidal flow over Camarinal Sill, Strait of Gibraltar. Journal of Geophysical Research 116, C12026. http://dx.doi.org/10.1029/2011JC007093.

Sanz, J.L., Acosta, J., Esteras, M., Herranz, P., Palomo, C., Sandoval, N., 1991. Prospección geofísica del Estrecho de Gibraltar: resultados del programa Hércules (1980–1983). Publicaciones Especiales del Instituto Espanol de Oceanografia, 7–48.

Speich, S., 1996. A Strait outflow circulation process study: the case of the Alboran Sea. Journal of Physical Oceanography 26, 320–340.

Tintoré, J., Gomis, D., Alonso, S., Parrilla, G., 1991. Mesoscale dynamics and vertical motion in the Alborán Sea. Journal of Physical Oceanography 21, 811–823.

Tonani, M., Pinardi, N., Dobricic, S., Pujol, I., Fratianni, C., 2008. A high-resolution free-surface model of the Mediterranean Sea. Ocean Science 4, 1–14.

Vargas-Yáñez, M., Plaza, F., García-Lafuente, J., Sarhan, T., Vargas, J.M., Vélez-Belchí, P., 2002. About the seasonal variability of the Alboran Sea circulation. Journal of Marine Systems 35, 229–248.

Vélez-Belchí, P., Vargas-Yáñez, M., Tintoré, J., 2005. Observation of a western Alborán gyre migration event. Progress in Oceanography 66, 190–210.

Viúdez, A., Pinot, J.M., Haney, R.L., 1998. On the upper layer circulation in the Alboran Sea. Journal of Geophysical Research 103 (C10), 21,653–21,666. http://dx.doi.org/10.1029/98JC01082.

Whitehead, J.A., Miller, A.R., 1979. Laboratory simulation of the gyre in the Alboran Sea. Journal of Geophysical Research 84 (C7), 3733–3742. http://dx.doi.org/10.1029/JC084iC07p03733.